CHEMISTRY
A European Journal

www.chemeurj.org

Reprint

A Journal of
ChemPubSoc Europe
ACES
Asian Chemical Editorial Society
WILEY-VCH

ChemPubSoc Europe

DOI: 10.1002/chem.201806186

CHEMISTRY A European Journal Full Paper

Heterogeneous Catalysis |*Hot Paper*|

"Click" Silica-Supported Sulfonic Acid Catalysts with Variable Acid Strength and Surface Polarity

Palraj Kasinathan,[a] Charlotte Lang,[a] Sambhu Radhakrishnan,[b] Josefine Schnee,[a] Cécile D'Haese,[a] Eric Breynaert,[b] Johan A. Martens,[b] Eric M. Gaigneaux,[a] Alain M. Jonas,[a] and Antony E. Fernandes*[a, c]

Abstract: Solid acid catalysts are central in our chemical industry and are major players in the valorization of bioresources. However, there is still a need to develop solid acid catalysts with enhanced acid strength and improved, or tunable, physicochemical profile to enhance the efficiency and sustainability of chemical processes. Here, a modular approach to tune the acid strength and surface polarity of silica-supported sulfonic acid catalysts, based on a versatile copper-catalyzed azide–alkyne cycloaddition (CuAAC)-based anchoring scheme, is presented. The CuAAC-formed triazole link was used to enhance the activity of the grafted sulfonic acids and to pair the acid sites with secondary hydrophobic functions. The beneficial effects of both the triazolium link and the paired hydrophobic site, as well as the optimal positioning of the sulfonic moiety on the triazole ring, are discussed in model esterification reactions.

Introduction

Acid catalysis is arguably one of the most important areas of catalysis, with extensive applications in key chemical transformations, such as dehydration, hydrolysis, alkylation or esterification, and is becoming critical for biomass conversion.[1] Strong mineral acids, such as the widely used sulfuric acid, are however generally associated with several drawbacks including safety hazards, equipment corrosion, cost of disposal, waste management, and environmental concerns, which drastically constrain their applications in industry, in which more sustainable alternatives are preferred, or anticipated by more stringent environmental regulations. In this direction, the development of hybrid organic–inorganic acid catalysts in which the molecular acids are immobilized on a solid support has focused on merging the advantages of homogeneous and heterogeneous catalysis. For instance, mesoporous-silica-supported acids, such as the well-known propyl sulfonic acid silicas (SiPr-SO_3H),[2] have been employed with success in many examples.[3] Yet, the performances of organosulfonic-acid-functionalized mesoporous silica, and solid acid catalysts in general, are often governed by the transport and adsorption of the reactants to and at the active sites, as well as by the acid strength of these active sites. Indeed, the polar sulfonic acid groups are often hydrated or interacting with surface silanol groups, which contributes to a significant decrease of their acid strength.[4] Likewise, the high polarity of the sulfonic-acid-functionalized silica surface could also be detrimental to the efficient transport of reactants and products, and can lead to fast deactivation, especially in the case in which water is used as a solvent, reactant, or formed as a by-product.[5] The development of solid acid catalysts with controllable acid strength and polarity is therefore a major challenge, which would unlock a full range of new opportunities.[6] Controlling the hydrophilic–hydrophobic balance of catalytic surfaces provides handles to increase the acid strength by desolvating the silica surface and the acid sites from water (as a by-product, solvent or initially physisorbed at the silica surface), and to develop water-tolerant catalytic systems.[3c,4,7] This design principle also serves for optimizing the diffusion and adsorption of less polar reactants to the acid sites to achieve enhanced catalytic activity and selectivity.[3b–d,8] Similarly, it could serve to shift reaction equilibrium by expelling products, or by-products, from the active sites.[9] Hence, it becomes critical to develop methods allowing for the rational design and preparation of solid acid catalysts with controllable acid strength and physicochemical properties.

Here, we disclose an efficient strategy to prepare silica-supported sulfonic acid catalysts with controllable acid strength and surface polarity, taking advantage of the highly modular copper-catalyzed azide–alkyne cycloaddition (CuAAC) chemistry. We show that the triazole anchor, resulting from the CuAAC-grafting of the sulfonic acid to the azide-functionalized

[a] *Dr. P. Kasinathan, Dr. C. Lang, Dr. J. Schnee, C. D'Haese, Prof. E. M. Gaigneaux, Prof. A. M. Jonas, Dr. A. E. Fernandes*
Institute of Condensed Matter and Nanosciences, UCLouvain
1348 Louvain-la-Neuve (Belgium)

[b] *Dr. S. Radhakrishnan, Dr. E. Breynaert, Prof. J. A. Martens*
Center for Surface Chemistry and Catalysis
Characterization and Application Team
KULeuven, 3001 Leuven (Belgium)

[c] *Dr. A. E. Fernandes*
Current address: Certech
Rue Jules Bordet, 7180 Seneffe (Belgium)
E-mail: antony.fernandes@certech.be

Supporting information and the ORCID identification number(s) for the author(s) of this article can be found under: https://doi.org/10.1002/chem.201806186.

mesoporous silica surface, can serve to increase the acid strength and activity of the sulfonic acid when transformed into a triazolium. This inductive effect can be modulated by the nature of the secondary substituents on the triazole ring or by the spacing of the sulfonic acid site from the electron-withdrawing triazolium ring. Next to this, we extend the strategy to the preparation of silica-supported bifunctional catalysts incorporating paired sulfonic acids and hydrophobic hydrocarbon chains. The synergistic effects of both the triazolium link and the hydrophobic group are demonstrated in model esterification reactions.

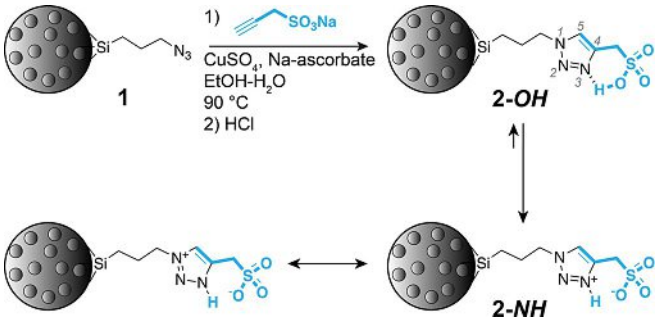

Scheme 1. CuAAC-grafting of sulfonic acid catalysts on mesoporous silica particles.

Results and Discussion

Tuning the acidity of silica-supported sulfonic acids

Mesoporous-silica-supported sulfonic acids, such as the well-known propyl sulfonic acid silicas (SiPr-SO_3H), are generally prepared from alkyl-thiol-functionalized silicas.[2a,10] The later are either obtained by direct or post-synthesis methods using a mercaptosilane. The oxidation of the thiol-terminated monolayer and subsequent acidification provide the alkyl sulfonic acid mesoporous silica. However, this well-established methodology has some drawbacks, such as the use of redox sensitive thiols and the need for an oxidation step, which can be detrimental to other redox-sensitive groups present on the surface in the case of multifunctional catalysts. Moreover, this oxidation step is often incomplete and leaves unreacted thiol groups on the surface.[10,11] To circumvent these limitations, we turned our attention to the copper-catalyzed azide–alkyne cycloaddition (CuAAC) for the direct covalent grafting of sulfonic acid groups on silica (Scheme 1).

The CuAAC post-functionalization method has become a method of choice for the grafting of most types of homogeneous catalysts, both organic and organometallic ones, under benign conditions and almost quantitative yields on a large variety of supports.[12] Alternatively, a most notable advantage of the CuAAC reaction in the field lies in its unique potential towards the preparation of multifunctional supported catalysts, in part due to its high efficiency and large functional group tolerance. Multifunctional supported catalysts have recently opened new possibilities in cooperative and cascade catalysis, with activities that can surpass that of the parent homogeneous catalysts.[13] However, the need to immobilize and accommodate multiple catalytically active functional groups on a single support is particularly challenging from a synthetic point of view. This also adds to the necessity to precisely adjust their surface ratio, proximity and distribution to arrive at the full catalytic potential of these hybrid systems.[14] As such, the "click" CuAAC chemistry, by its very nature, is well suited for this purpose and has allowed for the simultaneous grafting of multiple catalytically active groups on silica with accurate control on their surface ratio and distribution.[12e,14a,b,15]

CuAAC-grafted sulfonic acid catalyst **2** was prepared by reaction of sodium propargylsulfonate with azide-modified mesoporous silica particles **1** (azide loading $= 0.27 \pm 0.06$ mmol g^{-1}) in the presence of Cu^{I} precursors at 90 °C (Scheme 1).[16] Thermogravimetric analysis (TGA) of functionalized silica **2** (Supporting Information, Figure S1) confirmed the efficient grafting of the sulfonated alkyne with an organic loading of 0.33 mmol g^{-1} (Table 1). In parallel, FTIR confirmed the complete disappearance of the typical azide band at 2100 cm^{-1} fol-

Table 1. Organic loadings, ion-exchange capacity (IEC) and textural properties.

Silica	Organic loading [mmol g^{-1}]	IEC [mmol g^{-1}]	BET surface area [$m^2 g^{-1}$]	Pore volume [$cm^3 g^{-1}$]	Pore diameter [nm]
1	0.27 ± 0.06	0.04	267	0.68	6.9
2	0.33 ± 0.01	0.38	195	0.55	6.7
3	0.29 ± 0.01	0.04	n.d.	n.d.	n.d.
4	0.35 ± 0.01	0.47	243	0.60	6.8
5	0.35 ± 0.01	0.70	234	0.60	6.7
6	0.32 ± 0.01	0.39	233	0.60	6.8
7	0.39 ± 0.01	0.84	209	0.50	6.7
SiPr-SO_3H	0.47 ± 0.11	0.66	277	0.57	6.6
8	0.33 ± 0.01	0.04	218	0.53	6.3
9	0.30 ± 0.01	0.08	205	0.45	5.9
10	0.32 ± 0.01	0.45	175	0.40	5.6
11	0.35 ± 0.01	0.04	221	0.49	6.2
12	0.36 ± 0.01	0.46	168	0.40	6.0
13	0.36 ± 0.01	0.45	158	0.38	5.9
14	0.25 ± 0.01	0.32	222	0.57	6.8
15	0.25 ± 0.01	0.31	244	0.66	7.3

lowing the CuAAC reaction of propargylsulfonate with azide-silica **1** (Supporting Information, Figure S3). XPS of **2** also verified the appearance of a S 2s signal at 232.5 eV, consistent with oxidized sulfur (Supporting Information, Figure S6, Table S3).[17]

Solid-state ^{13}C NMR spectra were recorded by using a multiple-contact cross-polarization magic-angle spinning experiment (MC-CPMAS) with spinal64 decoupling. MC-CPMAS enables ^{13}C NMR characterization of materials containing carbon moieties at natural abundance and exhibiting highly different cross-polarization built-up properties. Using a sequence of multiple short contacts separated by repolarizing periods and storage of the longitudinal polarization along the *z*-axis, instead of using very long contact pulses like in a classic CPMAS experiment, all carbon moieties can be similarly polarized. The MC-CPMAS approach indeed prevents the decay of the signal due to $T_{1\rho}$ relaxation ($T_{1\rho}$ = spin–lattice relaxation in the rotating frame), leading to more internally quantitative representation of a sample containing differently relaxing species, hence delivering information similar to direct excitation spectra (Supporting Information, Figure S21). Figure 1a depicts the ^{13}C MC-CPMAS spectra of the azide modified silica **1** that shows 4 peaks in total, three of which corresponding to the carbons of the propyl group and the fourth, sharper peak associated with residual solvent, CH_2Cl_2.

Comparing the ^{13}C spectrum of the material modified by using the CuAAC reaction with propargylsulfonate **2** (Figure 1b) to the spectrum of **1**, two olefinic signals corresponding to carbons 4 and 5 are immediately noticed. The extra peak at approximately 46 ppm can be attributed to the CH_2 group close to the sulfonic acid function. Close inspection of the spectrum also reveals the presence of small amounts of CH_2Cl_2 (48.5 ppm) and DMF (peaks at 162, 36, and 31 ppm) solvents.

The density of acidic protons in **2** was measured by ion exchange capacity (IEC) with 2 M NaCl followed by acid–base titration, and was determined to be 0.38 mmol g^{-1} (Table 1), which is also consistent with the measured organic loading when due account is taken of the contribution from unsubstituted acidic silanol sites (0.04 mmol g^{-1}, Table 1, **1**). However, despite this measured acidity, catalyst **2** proved inefficient in catalyzing the model esterification of *n*-butanol with acetic acid at a 0.06 mol% catalyst loading; **2** proceeded in a similar way to the autocatalyzed (blank) reaction (Figure 2a). Alternatively, under identical reaction conditions, commercial propyl sulfonic acid silica (SiPr-SO_3H, IEC = 0.66 mmol g^{-1}, Table 1), lacking the triazole moiety, proved efficient in catalyzing the reaction (Figure 2a). This observation clearly pointed towards a negative effect of the triazole linker.

The pK_{BH^+} values of 1,4-disubstituted 1,2,3-triazoles is approximately 0 in water,[18] whereas alkyl sulfonic acids have a typical pK_a of about -2.[19] Although measuring pK_a values for solid acids is difficult, it can be assumed that the relative acidity constants of the supported molecular species are in the same range than their corresponding free forms in solution, which hence accounts for a relatively fast proton transfer from the sulfonic acid to the N3-nitrogen of the triazole ring,[18] with

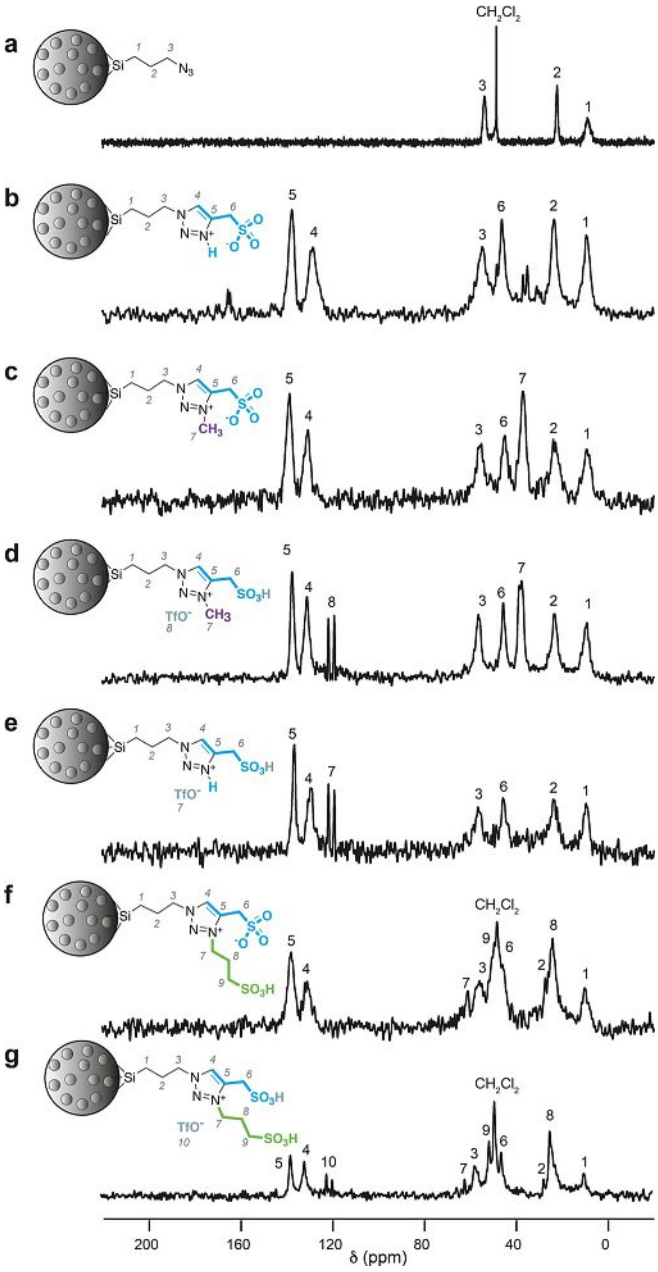

Figure 1. ^{13}C MC-CPMAS NMR spectra of silica a) **1**, b) **2**, c) **3**, d) **4**, e) **5**, f) **6** and g) **7**.

an equilibrium constant $K_{eq} \approx 10^2$, this being further facilitated by a 6-membered ring triazole–sulfonic-acid hydrogen-bond system (Scheme 1). Hence, this suggests that catalyst **2-*OH*** exists predominantly in its stable triazolium zwitterionic form **2-*NH*** (Scheme 1), which is obviously not strongly acidic anymore to catalyze the esterification reaction.

Analysis of the high-resolution N 1s XPS spectrum of **2** showed the appearance of an uncommon high-energy peak at 402.1 eV together with another peak at 400.2 eV in an approximately 2:1 ratio (Figure 3a and Table S3 in the Supporting Information). This observation is consistent with 1,2,3-triazolium species characterized by electron-deficient N1- and N3-nitrogen atoms (Scheme 1),[20] thus confirming the structure **2-*NH***.

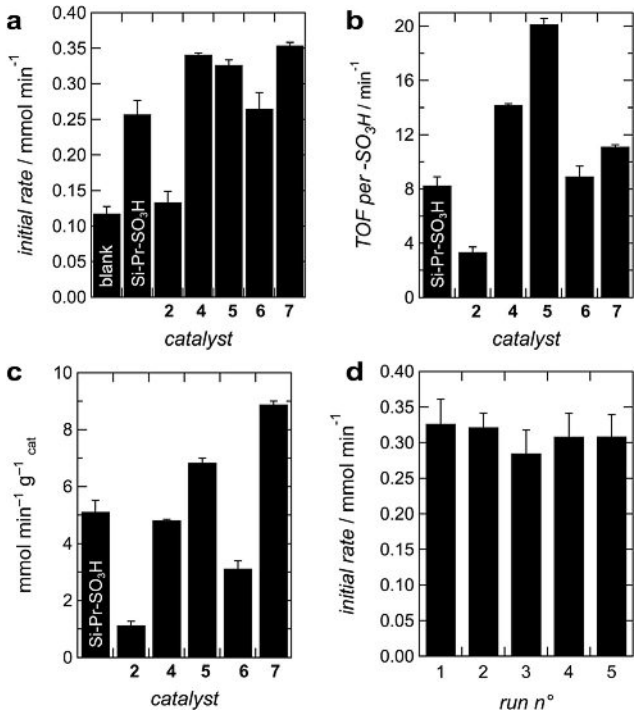

Figure 2. a) Catalytic activity of **2**, **4**, **5**, **6** and **7** in the esterification of *n*-butanol with acetic acid, compared to the autocatalyzed reaction (blank) and a commercial propylsulfonic acid silica (SiPr-SO_3H). b) TOFs per -SO_3H. c) Mass activity. d) Recycling of catalyst **5**.

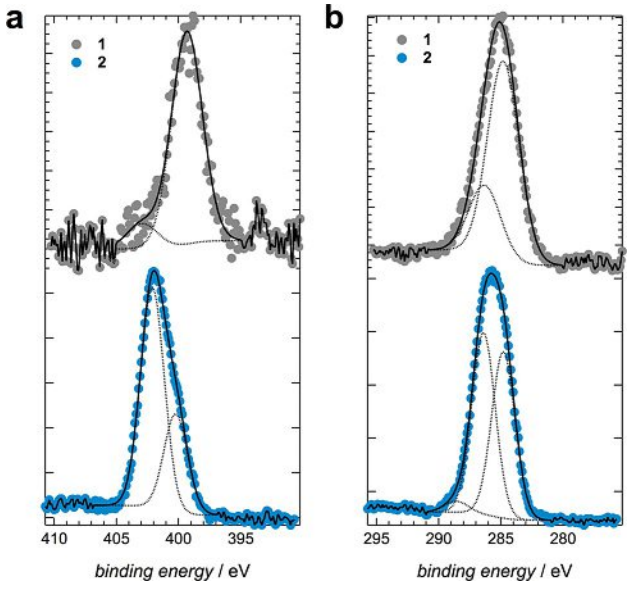

Figure 3. High-resolution a) N 1s and b) C 1s XPS spectra of **1** and **2**.

Alternatively, the high-resolution C 1s XPS spectrum of **2** showed an increase of the high energy C 1s component at 286.4 eV in reference to azide-functionalized silica **1** (Figure 3 b). This corresponds to the additional electron-poor triazolium carbons in **2** originating from the propargyl sulfonic moiety, which is again consistent with the triazolium structure ***2-NH***.

This finding that the CuAAC approach is a priori not suitable for the grafting of strong Brønsted acids without depleting their catalytic properties adds to the few limitations of the CuAAC method for the covalent immobilization of molecular catalysts.[21] Based on this understanding, we hypothesized that blocking the slightly basic character of the CuAAC-formed triazole linker might prevent this neutralization and permit to maintain the activity of the grafted sulfonic acid moiety. One such possibility is to *N*-alkylate the triazole ring to give a triazolium salt lacking any basic/nucleophilic capacity.[22] Following reported procedures,[23] functionalized silica **2** was treated with excess methyl iodide in acetonitrile at 90 °C. However, after submitting **2** to these conditions, the absence of a new thermal event in TGA (Supporting Information, Figure S1 a) indicated that the targeted reaction did not occur. This is consistent with the triazole being already protonated and, thus, not capable of nucleophilic reaction with methyl iodide. Hence, the modification of **2** was repeated in presence of the base *N*,*N*′-diisopropylethylamine (DIPEA; $pK_{BH^+} = 11$) to deprotonate the triazole ring and enable its *N*-methylation at the N3-nitrogen position (Scheme 2). Under these circumstances, **3** was obtained with a grafting density of 0.30 mmol g^{-1} (Table 1); this again confirmed our hypothesis of the triazole being protonated in **2**. XPS of **3** also showed high-energy N 1s nitrogen peak at 402.3 eV corresponding to 1,2,3-triazolium species (Supporting Information, Figure S8). The ^{13}C MC-CPMAS spectrum of **3** (Figure 1 c), exhibits a new peak at approximately 37 ppm, confirming the *N*-methylation at the N3-nitrogen atom.

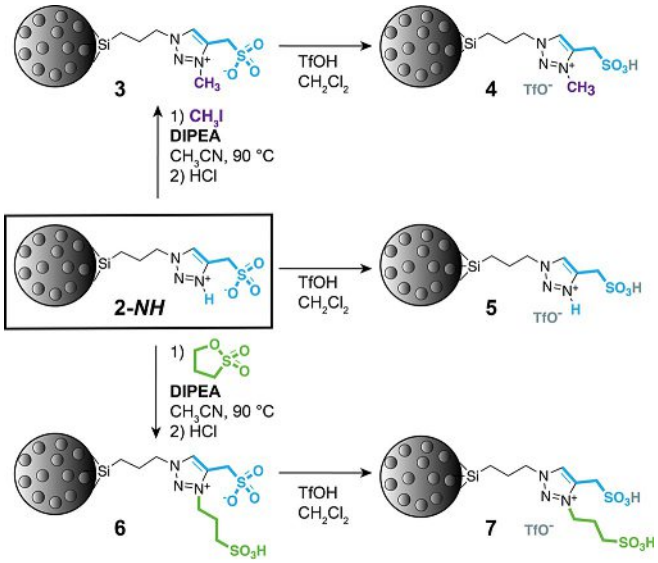

Scheme 2. Preparation of silica-supported triazolium catalysts **4**, **5**,and **7**.

Zwitterionic silica **3** (IEC = 0.04 mmol g^{-1}) was then protonated with trifluoromethanesulfonic acid (TfOH), which possesses a sufficiently low pK_a (ca. −14) to afford the sulfonic acid catalyst **4**.[24] The presence of TfO^- in catalyst **4** was confirmed by the occurrence of two ^{13}C NMR peaks associated to triflate at 121.6 and 119 ppm (Figure 1 d), as well as by XPS analysis

showing F 1s and high-energy C 1s peaks (Supporting Information, Figures S6–S7).

Similarly, catalyst **5** was obtained by direct treatment of **2** with TfOH (Scheme 2). ^{13}C NMR and XPS analysis of **5** again confirmed the presence of the triflate anion (Figures 1e and Figures S6 and S7, Supporting Information). IEC measurements indicated proton loadings of 0.47 and 0.70 mmol g^{-1} for **4** and **5**, respectively (Table 1). Elemental analysis of **4** and **5** provided C/N atomic ratio of 2.7 and 2.4, in agreement with the nominal values of 2.7 and 2.3, respectively.

In a similar way, we turned our attention to the use of sultone electrophiles, which would advantageously allow to append an additional alkyl sulfonic acid moiety upon reaction with the triazole. Following methodologies used in the preparation of Brønsted acidic ionic liquids,[24a,c,e,25] **2** was treated with 1,3-propanesultone in toluene at 90 °C (Scheme 2). As previously, no reaction was observed by TGA in the absence of an extra base (Figure S1b, Supporting Information). Contrarily, performing the reaction in presence of DIPEA led to the efficient formation of the zwitterionic silica **6** (Table 1), with a grafting density of 0.32 mmol g^{-1}. As expected, XPS of **6** showed a nitrogen N 1s peak at 402.1 eV (Figure S8, Supporting Information). IEC analysis gave a proton loading of 0.39 mmol g^{-1} for **6** that upon protonation with TfOH increased to 0.84 mmol g^{-1}. Elemental analysis of **7** provided a C/N atomic ratio of 3.5, in agreement with the nominal value of 3.3. Functionalization with a propyl sulfonic acid group and its subsequent protonation by triflic acid was confirmed by solid-state NMR, as revealed in Figure 1f,g for **6** and **7**, respectively.

Catalysts **4**, **5**, and **7** were similarly evaluated in the esterification of *n*-butanol with acetic acid at a catalyst loading of 0.06 mol% and showed activity 30 to 40% higher than with the commercial SiPr-SO_3H (Figure 2a). In parallel, zwitterionic catalyst **6** showed inferior activity compared to the other solid acid triazolium catalysts, with an initial reaction rate identical to SiPr-SO_3H (Figure 2a). The highest turnover frequency (TOF) per -SO_3H was attained with catalyst **5** (TOF = 20 min^{-1}), 2.5 times higher than with the commercial sulfonic acid silica (Figure 2b). When normalized by the mass unit of silica catalyst, catalysts **4**, **5**, and **7** proved similar or more efficient than commercial SiPr-SO_3H, with **7** culminating with an almost two-fold enhanced activity (Figure 2c).

These overall observations underpin the presence of sulfonic acid protons of different acid strengths, obviously influenced by the presence of the triazolium cation. Indeed, the electron-withdrawing triazolium ring increases the acid strength of the vicinal sulfonic acid through strong inductive effects, with acidity that can decrease by 2–3 pK_a units, as previously demonstrated with carboxylic-acid-functionalized imidazolium ionic liquids.[26] Hence, the different acidic protons found in the supported catalysts can be ordered as follows: (triazolium)N^+–H (**2**) ⋘ propyl-SO_3H (SiPr-SO_3H) < CH_3-triazolium-CH_2-SO_3H (**4**) < H-triazolium-CH_2-SO_3H (**5**)—the donor effect of the methyl group reduces the electronegativity of the triazolium in **4** compared to **5**. Inductive effects rapidly decrease with distance, which explains the lower activity of **6** compared to the other triazolium catalysts **4**, **5** and **7**; **6** shows an activity, hence acidity, similar to a conventional propyl sulfonic acid as in SiPr-SO_3H (Figure 2a). To provide further evidence for these effects, potentiometric titrations with *n*-butylamine were performed (Supporting Information, Figure S22). The initial electrode potential E_i (Figure 4a) provided an indication of the acid strength of the different solid catalysts[27] that confirmed our classification.

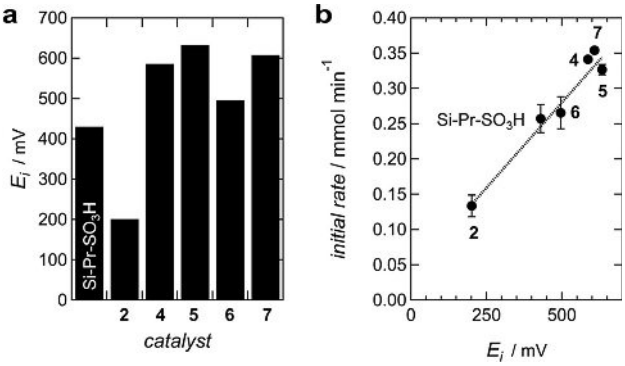

Figure 4. a) Initial electrode potential (E_i) of **2**, **4**, **5**, **6**, **7** and SiPr-SO_3H obtained by potentiometric titration with *n*-butylamine. b) Initial reaction rate vs. initial electrode potential (E_i).

Catalyst **5** showed the highest E_i of 633 mV, slightly superior to catalysts **4** (586 mV) and **7** (608 mV), whereas the lowest value was measured for **2** (201 mV). Remarkably, the E_i values correlated well with the measured initial reaction rates (Figure 4b). Catalyst **5** could be simply recovered and reused for **5** consecutive runs without significant loss of activity, demonstrating the benefit of catalyst immobilization (Figure 2d).

Tuning the hydrophobicity of silica-supported sulfonic acids

Controlling the surface hydrophobicity of sulfonic acid silicas is attainable either by co-condensation of a mercaptosilane and an alkylsilane[10,28] or by post-functionalization of the alkyl sulfonic acid silica with an hydrophobic organosilane.[8b] These approaches could easily be transposed to our CuAAC methodology by either co-grafting (or co-condensing) the azidopropyltrimethoxysilane with a secondary silane,[16e,29] or possibly by a CuAAC post-functionalization route using a mix of alkynes.[12e,14a,b,15] However, the main limitation of these approaches is that the sulfonic acid and secondary hydrophobic groups would be randomly distributed on the silica surface; a situation that can restrict a rational interpretation of the effect of the secondary group on catalytic properties. For instance, Davis and co-workers have shown that bifunctional catalysts comprising paired cooperative catalytic groups can achieve enhanced activity and selectivity in comparison to the corresponding randomly distributed bifunctional catalysts.[30] Hence, we reasoned that using the triazole ring as an anchoring point for both the sulfonic acid site and the secondary group, resulting in a paired catalytic system, would benefit to a better control and interpretation of the local interactions at the active site.

Following our approach, the spectator hydrophobic segment can either be installed at the C4- or N3-position of the triazole depending whether it is introduced by the CuAAC reaction or by the alkylation of the CuAAC-formed triazole, respectively (Scheme 3). From the above observations, stronger acidity and activity should be obtained when the sulfonic acid site is located closer to the triazolium to benefit from its strong electron-withdrawing inductive effect.

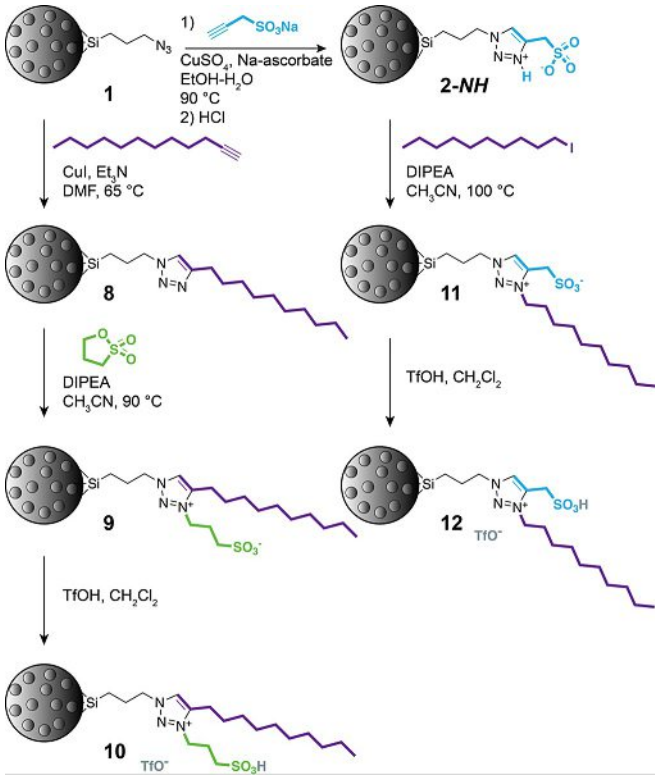

Scheme 3. Preparation of bifunctional catalysts **10** and **12** bearing paired sulfonic acid and hydrophobic functions.

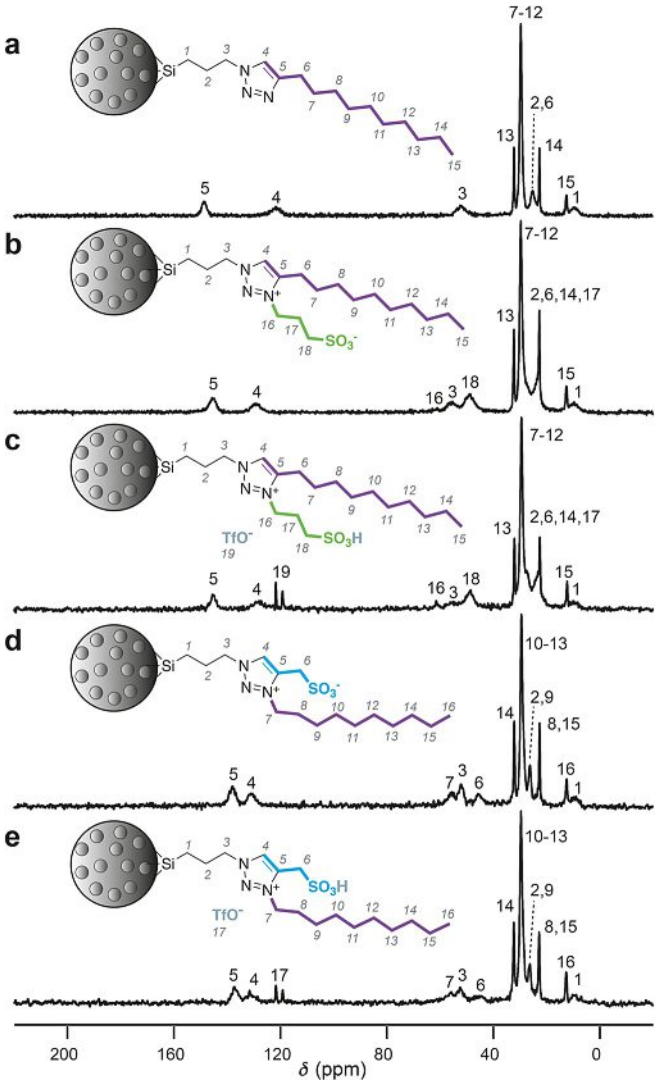

Figure 5. ^{13}C NMR spectra of silica a) **8**, b) **9**, c) **10**, d) **11**, and e) **12**.

Sulfonic acid catalysts **10** and **12**, which have either a hydrophobic decyl group at the C4- or N3-position of the triazole, respectively, were prepared from azide-functionalized mesoporous silica (Scheme 3). Catalyst **10** was obtained by first reacting silica **1** with 1-dodecyne in presence of CuI and Et_3N, our typical CuAAC conditions,[12e,14a,b,15] providing **8**. The sulfonic acid function in **10** was then introduced by alkylation of the triazole ring with propanesultone followed by protonation of the sulfonate with TfOH by using the sequence developed for catalyst **7**. In parallel, catalyst **12** was prepared through alkylation of CuAAC-immobilized sulfonic acid silica **2** with excess 1-iododecane followed by acidification with TfOH by using a synthetic route identical to that of catalyst **4**. The organic loadings, IEC and textural properties of the bifunctional catalysts are reported in Table 1. Elemental analysis of **10** and **12** provided C/N atomic ratio of 5.8 and 5.5, consistent with the nominal values of 6.3 and 5.7, respectively. As shown in Figure 5 a–e, the modifications leading to catalysts **8** to **12** were consistently confirmed by the ^{13}C MC-CPMAS spectra of these materials.

Catalysts **10** and **12** were tested in the esterification of *n*-octanol with acetic acid at a catalyst loading of 0.1 mol% and compared with catalysts **4**, **5** and **7** as well as with the commercial propylsulfonic acid silica and the autocatalyzed (blank) reaction (Figure 6 a). As expected, bifunctional catalysts **10** and **12** outperformed catalysts **4**, **5** and **7**, with a 1.5-to-2-fold increase in the initial reaction rates. Impressively, the esterification of octanol using the commercial SiPr-SO_3H silica appeared extremely slow under the same reaction conditions, with an initial reaction rate of 0.07 mmol min^{-1}, approximately 5-fold inferior to that of the CuAAC-immobilized sulfonic acid catalysts **10** and **12** incorporating a secondary hydrophobic segment. Additionally, catalyst **12** exhibited a 25% higher initial reaction rate than catalyst **10**; the latter, having the sulfonic acid located three carbons away from the triazole instead of only one carbon in **12**, experiences a much lower influence from the electron-withdrawing triazolium ring. The potentiometric titration of **10** and **12** with *n*-butylamine supported this observation with initial electrode potentials of 589 and 660 mV (Table S4, Supporting Information), respectively, which confirms

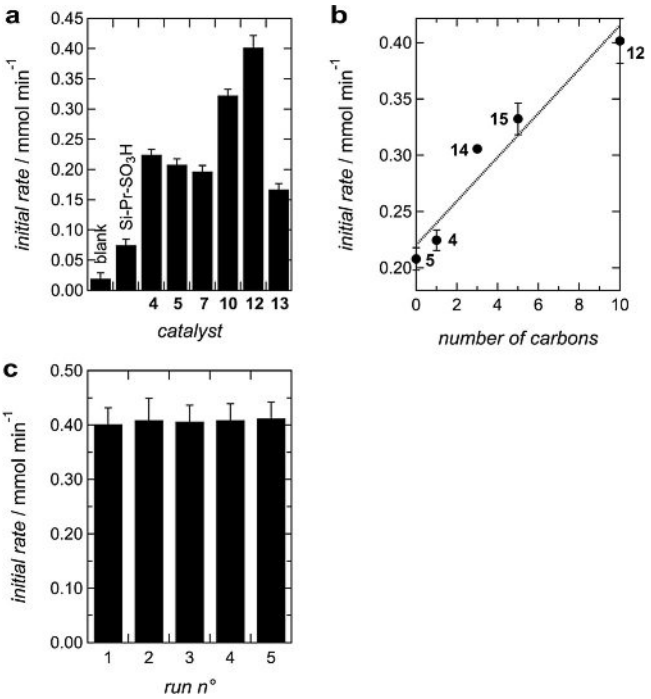

Figure 6. a) Catalytic activity of **4**, **5**, **7**, **10**, **12**, and **13** in the esterification of *n*-octanol with acetic acid, compared to the autocatalyzed reaction (blank) and a commercial propylsulfonic acid silica (SiPr-SO_3H). b) Initial reaction rate as a function of the number of carbons in the secondary hydrophobic chains. c) Recycling of catalyst **12**.

a higher acid strength of the sulfonic acid in **12** imparted to the stronger effect of the triazolium ring, as expected.

To further evidence the synergistic effect of the secondary hydrophobic moiety in bifunctional sulfonic acid catalysts **10** and **12**, the bifunctional catalyst **13** (Figure 7) was prepared,

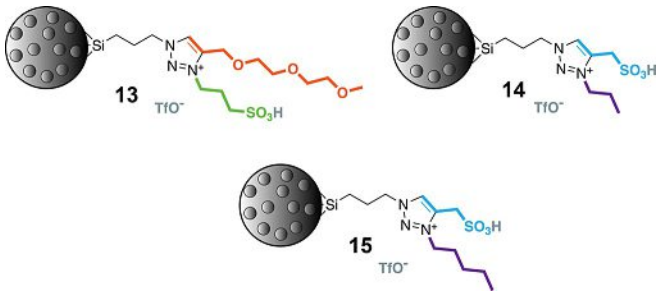

Figure 7. Structure of bifunctional silica-supported catalysts **13**, **14**, and **15**.

which incorporates a hydrophilic diethylene glycol methyl ether chain on the triazole ring instead of the hydrophobic decyl hydrocarbon chain of similar length. Catalyst **13** was synthesized following the route described for catalyst **10** (Scheme 3) by using the propargylated diethylene glycol methyl ether instead of 1-dodecyne. With the same idea, catalysts **14** and **15** (Figure 7), bearing shorter alkyl chains (propyl and pentyl, respectively) at the N3-position of the triazole, were prepared. Elemental analysis of **13**, **14**, and **15** provided C/N atomic ratio of 4.9, 3.3, and 3.9, consistent with the nominal values of 5.0, 3.3, and 4.0, respectively. As demonstrated by the spectra shown in Figure 8 a–c, ^{13}C MC-CPMAS NMR immediately reveals that the structural modifications leading up to catalysts **13** to **15** yielded phase pure structures. Indeed, in the NMR spectra only resonances resulting from the expected surface functionalization are visible.

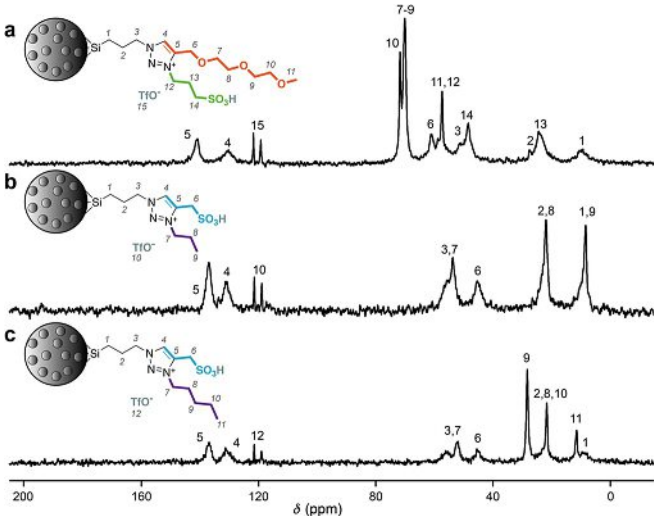

Figure 8. ^{13}C NMR spectra of silica a) **13**, b) **14**, and c) **15**.

As expected, catalysts **13** proved the least active catalyst in the esterification of *n*-octanol, even slower than catalysts **4**, **5**, and **7** (Figure 6 a). Remarkably, the initial reaction rates measured with supported sulfonic acid catalysts bearing hydrocarbon chains at the N3-position of the triazole (catalysts **4**, **12**, **14**, and **15**) linearly followed the length of the alkyl chains, in agreement with their increased hydrophobic character (Figure 6 b).

Conclusion

In summary, we have developed a simple method that offers considerable flexibility to tune both the acid strength and surface polarity of silica-supported sulfonic acid catalysts. Although the efficient CuAAC anchoring scheme appeared not suitable for the benign grafting of sulfonic acids on mesoporous silica, derivatization of the guilty basic triazole link into an electron-withdrawing triazolium ring enabled to restore and significantly boost the acidity of the proximal sulfonic acid by strong inductive effects. In addition, the triazole ring was used to prepare, in a very modular way, bifunctional catalysts comprising paired sulfonic acid and secondary groups to probe the effect of the local environment of the active site. We showed that the nature and relative position of the paired organic groups on the triazolium ring largely affected the catalytic performances of the system.

Our work, in addition to enabling the use of CuAAC for the grafting of the important class of strong Brønsted acid molecular catalysts, opens new routes towards the rational design and preparation of solid acid catalyst with controllable acid

strength and surface polarity, a design principle that is becoming critical for biomass valorization.

Experimental Section

General considerations

Reagents were obtained from commercial sources and used without further purification. All reactions were carried out under argon. Spherical silica gel (40–75 μm, 100 Å) was purchased from Sorbtech Technologies. Milli-Q water (resistivity 18.2 MΩ cm) was obtained from a Milli-Q Reference system (Merck). FTIR was measured on a Thermo Scientific FT-IR Nexus 870 spectrometer. TGA was measured on a Mettler Toledo TGA/SDTA 851e instrument. The weight loss was measured in the 150–900 °C temperature range. Specific surface area and pore size were obtained through nitrogen adsorption–desorption experiments using a Micromeritics Tristar 3000. Before the analysis, the samples were degassed overnight under vacuum at 150 °C. BET and BJH approaches were applied to process the raw data. X-ray photoelectron spectroscopy (XPS) measurements were performed on an SSX 100/206 photoelectron spectrometer from Surface Science Instruments equipped with a monochromatized microfocused Al X-ray source (1486.6 eV operated at 20 mA and 10 kV). All binding energies are referenced to the C-(C, H) component of the C 1s peak fixed at 284.8 eV. The base pressure in the spectrometer was in the low 10^{-8} torr range. Peak decomposition was achieved with Casa XPS (Casa Software Ltd., UK). Elemental analysis was performed on an EL cube apparatus. GC was performed on a Varian 3800 apparatus equipped with a CP-Sil8 CB column (30 m × 0.25 mm × 0.1 μm) and FID detector. ^{13}C NMR spectra were acquired on a Bruker 500 MHz Avance III spectrometer (11.74 T) equipped with a 4 mm H/X/Y triple channel probe head, using multiple-contact cross-polarization magic-angle spinning (MC-CPMAS)[31] with spinal64 ^{1}H decoupling at 55 kHz RF.[32] The samples were packed in a 4 mm ZrO_2 rotor and spun at 15 kHz. For MC-CPMAS, the t_z duration, which is the delay in the MC-CPMAS pulse sequence to allow for ^{13}C spin lattice relaxation between subsequent CP contact blocks, was set to 0.1 s, the individual CP contact duration to 0.5 ms, and the number of loops to 11 (total contact time of 5.5 ms). Spectra were referenced to the -CH peak of adamantane at 38.5 ppm (secondary reference), which was further referenced to tetramethylsilane (TMS) at 0 ppm as the primary reference.

Catalyst preparation

Preparation of azide-functionalized silica 1: Commercially available spherical silica (Sorbtech Technologies, 40–75 μm, 100 Å) was refluxed in 6 M HCl (10 mL g^{-1}) for 1 day. The silica was filtered and washed with milli-Q water until neutral pH and dried in oven for 2 days at 120 °C. The resulting silica was then placed in a round-bottomed flask and heated at 120 °C under vacuum for 6 hours. The flask was then allowed to cool to room temperature and toluene (20 mL g^{-1}) was added together with 3-azidopropyltrimethoxysilane (2 mmol g^{-1}) and the resulting mixture refluxed overnight. The silica was then filtered, washed with toluene, CH_2Cl_2, and finally dried in vacuum at 60 °C to give azide-functionalized silica **1**.

Preparation of catalyst 2: Azide-functionalized silica **1** was suspended in EtOH/water (2:1, 20 mL g^{-1}). Sodium propargylsulfonate (3 equiv. vs. N_3 loading) was added subsequently followed by sodium ascorbate (0.75 equiv) and $CuSO_4$ (0.625 equiv). The reaction was stirred overnight at 90 °C and monitored by FTIR and TGA. The functionalized silica was recovered by filtration and washed with DMF, water, 2 M HCl, MeOH, and CH_2Cl_2 and dried in vacuum at 60 °C overnight to afford catalyst **2**.

Preparation of catalyst 4: Catalyst **2** was suspended in CH_3CN (20 mL g^{-1}). CH_3I (20 equiv vs. triazole loading) was added followed by DIPEA (5 equiv) and the reaction was stirred at 100 °C for 2 days and monitored by TGA. The functionalized silica was recovered by filtration and washed with CH_3CN, water, 2 M HCl, MeOH, and CH_2Cl_2 and dried in vacuum at 60 °C overnight to afford **3**. Silica **3** was suspended in CH_2Cl_2 (20 mL g^{-1}), TfOH was added (1.05 equiv vs. triazole loading) and the reaction was stirred at room temperature for 4 hours. The functionalized silica was recovered by filtration, washed with CH_2Cl_2 and dried in vacuum at 60 °C overnight to afford catalyst **4**. Elemental analysis: C = 3.3 wt%, N = 1.4 wt%.

Preparation of catalyst 5: Catalyst **2** was suspended in CH_2Cl_2 (20 mL g^{-1}). TfOH (1.05 equiv vs. triazole loading) was added and the reaction was stirred at room temperature for 4 hours. The functionalized silica was recovered by filtration, washed with CH_2Cl_2 and dried in vacuum at 60 °C overnight to afford catalyst **5**. Elemental analysis: C = 2.9 wt%, N = 1.4 wt%.

Preparation of catalyst 7: Catalyst **2** was suspended in toluene (20 mL g^{-1}). 1,3-Propanesultone (5 equiv vs. triazole loading) was added followed by DIPEA (2 equiv) and the reaction was stirred at 90 °C for 1 day and monitored by TGA. The functionalized silica was recovered by filtration and washed with toluene, 2 M HCl, MeOH, and CH_2Cl_2 and dried in vacuum at 60 °C overnight to afford **6**. Silica **6** was suspended in CH_2Cl_2 (20 mL g^{-1}), TfOH was added (1.05 equiv vs. triazole loading) and the reaction was stirred at room temperature for 4 hours. The functionalized silica was recovered by filtration, washed with CH_2Cl_2, and dried in vacuum at 60 °C overnight to afford catalyst **7**. Elemental analysis: C = 4.0%, N = 1.3%.

Preparation of catalyst 10: Azide-functionalized silica **1** was suspended in degassed DMF (15 mL g^{-1}). 1-Dodecyne (1.5 equiv vs. azide loading) was added subsequently followed by Et_3N (5 equiv.) and CuI (0.1 equiv). The reaction was stirred overnight at 65 °C and monitored by FTIR and TGA. The functionalized silica was recovered by filtration and washed with DMF, water, 2 M HCl, MeOH, and CH_2Cl_2 and dried in vacuum at 60 °C overnight to afford silica **8**. Silica **8** was suspended in toluene (20 mL g^{-1}). 1,3-Propanesultone (5 equiv vs. triazole loading) was added followed by DIPEA (2 equiv.) and the reaction was stirred at 90 °C for 1 day and monitored by TGA. The functionalized silica was recovered by filtration and washed with toluene, 2 M HCl, MeOH, and CH_2Cl_2 and dried in vacuum at 60 °C overnight to afford **9**. Silica **9** was suspended in CH_2Cl_2 (20 mL g^{-1}), TfOH was added (1.05 equiv. vs. triazole loading) and the reaction was stirred at room temperature for 4 hours. The functionalized silica was recovered by filtration, washed with CH_2Cl_2, and dried in vacuum at 60 °C overnight to afford catalyst **10**. Elemental analysis: C = 8.5 wt%, N = 1.7 wt%.

Preparation of catalyst 12: Catalyst **2** was suspended in CH_3CN (20 mL g^{-1}). 1-Iododecane (50 equiv vs. triazole loading) was added followed by DIPEA (5 equiv) and the reaction was stirred at 100 °C for 3 days and monitored by TGA. The functionalized silica was recovered by filtration and washed with CH_3CN, water, 2 M HCl, MeOH, and CH_2Cl_2 and dried in vacuum at 60 °C overnight to afford **11**. Silica **11** was then suspended in CH_2Cl_2 (20 mL g^{-1}), TfOH was added (1.05 equiv vs. triazole loading) and the reaction was stirred at room temperature for 4 hours. The functionalized silica was recovered by filtration, washed with CH_2Cl_2 and dried in vacuum at 60 °C overnight to afford catalyst **12**. Elemental analysis: C = 6.7 wt%, N = 1.4 wt%.

Preparation of catalyst 13: Azide-functionalized silica **1** was suspended in degassed DMF (15 mL g^{-1}). Propargylated diethylene glycol methyl ether (1.5 equiv vs. azide loading) was added subsequently followed by Et_3N (5 equiv) and CuI (0.1 equiv). The reaction was stirred overnight at 65 °C and monitored by FTIR and TGA. The functionalized silica was recovered by filtration and washed with DMF, water, 2 M HCl, MeOH, and CH_2Cl_2 and dried in vacuum at 60 °C overnight to afford **S13a** (see Supporting Information). Silica **S13a** was suspended in toluene (20 mL g^{-1}). 1,3-Propanesultone (5 equiv vs. triazole loading) was added followed by DIPEA (2 equiv) and the reaction was stirred at 90 °C for 1 day and monitored by TGA. The functionalized silica was recovered by filtration and washed with toluene, 2 M HCl, MeOH, and CH_2Cl_2 and dried in vacuum at 60 °C overnight to afford **S13b**. Silica **S13b** was suspended in CH_2Cl_2 (20 mL g^{-1}), TfOH was added (1.05 equiv vs. triazole loading) and the reaction was stirred at room temperature for 4 hours. The functionalized silica was recovered by filtration, washed with CH_2Cl_2 and dried in vacuum at 60 °C overnight to afford catalyst **13**. Elemental analysis: C = 7.0 wt%, N = 1.7 wt%.

Preparation of catalyst 14: Catalyst **2** was suspended in CH_3CN (20 mL g^{-1}). 1-Iodopropane (40 equiv vs. triazole loading) was added followed by DIPEA (5 equiv) and the reaction was stirred at 100 °C for 2 days and monitored by TGA. The functionalized silica was recovered by filtration and washed with CH_3CN, water, 2 M HCl, MeOH, and CH_2Cl_2 and dried in vacuum at 60 °C overnight to afford **S14** (see Supporting Information). Silica **S14** was suspended in CH_2Cl_2 (20 mL g^{-1}), TfOH was added (1.05 equiv vs. triazole loading) and the reaction was stirred at room temperature for 4 hours. The functionalized silica was recovered by filtration, washed with CH_2Cl_2 and dried in vacuum at 60 °C overnight to afford catalyst **14**. Elemental analysis: C = 3.2 wt%, N = 1.1 wt%.

Preparation of catalyst 15: Catalyst **2** was suspended in CH_3CN (20 mL g^{-1}). 1-Iodopentane (40 equiv vs. triazole loading) was added followed by DIPEA (5 equiv) and the reaction was stirred at 100 °C for 2 days and monitored by TGA. The functionalized silica was recovered by filtration and washed with CH_3CN, water, 2 M HCl, MeOH, and CH_2Cl_2 and dried in vacuum at 60 °C overnight to afford **S15** (see Supporting Information). Silica **S15** was suspended in CH_2Cl_2 (20 mL g^{-1}), TfOH was added (1.05 equiv vs. triazole loading) and the reaction was stirred at room temperature for 4 hours. The functionalized silica was recovered by filtration, washed with CH_2Cl_2, and dried in vacuum at 60 °C overnight to afford catalyst **15**. Elemental analysis: C = 3.7 wt%, N = 1.1 wt%.

Methods

Ion-exchange capacity: Ion-exchange capacity (IEC) was determined by acid–base titration. Typically, the functionalized silica (ca. 100 mg) was dispersed in 2 M NaCl (10 mL) and stirred at 20 °C for 1 day. After decantation, the resulting solution was titrated with 5 mM NaOH in presence of phenolphthalein as the indicator.

Potentiometric titration: Potentiometric titration was performed with Hanna HI 991 002 Digital pH–mV model using a pH/ORP electrode. The dry solid catalysts (ca. 100 mg) was suspended in acetonitrile (10 mL) and agitated for 3 h. The suspension was then titrated with 5 mM *n*-butylamine.

Catalysis: The esterification reactions were carried out in a 50 mL round-bottomed flask equipped with a reflux condenser. Before the reaction, the catalysts were activated at 105 °C for 6 hours. The conversions were determined by GC analysis using reference samples. The initial reaction rates were determined by fitting the corresponding experimental data at low conversions with a linear function passing through the origin.

Butanol esterification: In a typical run, acetic acid (25.9 g, 0.43 mol) and the catalyst (0.06 mol%) were charged into the flask and heated to the reaction temperature (83 °C). On attaining the desired temperature, *n*-butanol (4 g, 0.05 mol) was introduced into the reaction mixture and this moment was considered as the zero reaction time. Samples were collected at regular intervals and analyzed by gas chromatography.

Octanol esterification: In a typical run, acetic acid (5.54 g, 0.09 mol) and the catalyst (0.1 mol%) were charged into the flask and heated to the reaction temperature (83 °C). On attaining the desired temperature, *n*-octanol (4 g, 0.03 mol) was introduced into the reaction mixture and this moment was considered as the zero reaction time. Samples were collected at regular intervals and analyzed by gas chromatography.

Acknowledgements

The authors acknowledge the European Regional Development Fund (ERDF) and Wallonia (Operational Program "Wallonia-2020.EU"), the Belgian Federal Science Policy (IAP P7/05), the Région wallonne-DG06 (Beware "Friedelcat" project n°1510459) and UCLouvain (teaching assistant–PhD student position of J.S.). Claudine Givron is acknowledged for elementary analysis measurements. S.R., E.B. and J.A.M. would like to express their gratitude concerning financial support by Research Foundation Flanders (FWO) through project funding (G.0885.14N). NMR equipment was acquired with financial support from the Hercules Foundation (AKUL/13/21), and by the Flemish Government, department EWI through the Hermes Fund (AH.2016.134). J.A.M. acknowledges the Flemish Government for long-term structural funding (Methusalem).

Conflict of interest

The authors declare no conflict of interest.

Keywords: bifunctional catalysts · click chemistry · esterification · sulfonic acid · supported catalysts

[1] a) A. Corma, H. García, *Chem. Rev.* **2003**, *103*, 4307–4366; b) G. Busca, *Chem. Rev.* **2007**, *107*, 5366–5410; c) F. Su, Y. Guo, *Green Chem.* **2014**, *16*, 2934–2957; d) P. Gupta, S. Paul, *Catal. Today* **2014**, *236*, 153–170.

[2] a) J. A. Melero, R. van Grieken, G. Morales, *Chem. Rev.* **2006**, *106*, 3790–3812; b) F. Hoffmann, M. Cornelius, J. Morell, M. Froba, *Angew. Chem. Int. Ed.* **2006**, *45*, 3216–3251; *Angew. Chem.* **2006**, *118*, 3290–3328; c) S. Rostamnia, E. Doustkhah, *RSC Adv.* **2014**, *4*, 28238–28248; d) G. Mohammadi Ziarani, N. Lashgari, A. Badiei, *J. Mol. Catal. A* **2015**, *397*, 166–191; e) B. Karimi, H. M. Mirzaei, A. Mobaraki, H. Vali, *Catal. Sci. Technol.* **2015**, *5*, 3624–3631; f) M. Ferré, R. Pleixats, M. Wong Chi Man, X. Cattoen, *Green Chem.* **2016**, *18*, 881–922.

[3] a) A. Karam, Y. Gu, F. Jerome, J.-P. Douliez, J. Barrault, *Chem. Commun.* **2007**, 2222–2224; b) Y. Gu, A. Karam, F. Jérôme, J. Barrault, *Org. Lett.* **2007**, *9*, 3145–3148; c) B. Karimi, D. Zareyee, *Org. Lett.* **2008**, *10*, 3989–3992; d) B. Karimi, A. Mobaraki, H. M. Mirzaei, D. Zareyee, H. Vali, *ChemCatChem* **2014**, *6*, 212–219; e) B. Lu, S. An, D. Song, F. Su, X. Yang, Y. Guo, *Green Chem.* **2015**, *17*, 1767–1778.

[4] J.-P. Dacquin, H. E. Cross, D. R. Brown, T. Duren, J. J. Williams, A. F. Lee, K. Wilson, *Green Chem.* **2010**, *12*, 1383–1391.

[5] T. Okuhara, *Chem. Rev.* **2002**, *102*, 3641–3666.

[6] F. Liu, K. Huang, A. Zheng, F.-S. Xiao, S. Dai, *ACS Catal.* **2018**, *8*, 372–391.

[7] a) P. L. Dhepe, M. Ohashi, S. Inagaki, M. Ichikawa, A. Fukuoka, *Catal. Lett.* **2005**, *102*, 163 – 169; b) A. Karam, J. C. Alonso, T. I. Gerganova, P. Ferreira, N. Bion, J. Barrault, F. Jérôme, *Chem. Commun.* **2009**, 7000 – 7002.

[8] a) I. Díaz, C. Márquez-Alvarez, F. Mohino, J. N. Pérez-Pariente, E. Sastre, *J. Catal.* **2000**, *193*, 295 – 302; b) I. K. Mbaraka, B. H. Shanks, *J. Catal.* **2005**, *229*, 365 – 373; c) A. Mobaraki, B. Movassagh, B. Karimi, *ACS Comb. Sci.* **2014**, *16*, 352 – 358.

[9] a) C.-H. Tsai, H.-T. Chen, S. M. Althaus, K. Mao, T. Kobayashi, M. Pruski, V. S. Y. Lin, *ACS Catal.* **2011**, *1*, 729 – 732; b) C. Swalus, B. Farin, F. Gillard, M. Devillers, E. M. Gaigneaux, *Catal. Commun.* **2013**, *37*, 80 – 84.

[10] D. Margolese, J. A. Melero, S. C. Christiansen, B. F. Chmelka, G. D. Stucky, *Chem. Mater.* **2000**, *12*, 2448 – 2459.

[11] W. M. Van Rhijn, D. E. De Vos, B. F. Sels, W. D. Bossaert, *Chem. Commun.* **1998**, 317 – 318.

[12] a) A. E. Fernandes, A. M. Jonas, O. Riant, *Tetrahedron* **2014**, *70*, 1709 – 1731; b) C. Ayats, A. H. Henseler, E. Dibello, M. A. Pericàs, *ACS Catal.* **2014**, *4*, 3027 – 3033; c) S. Ranjbar, P. Riente, C. Rodríguez-Escrich, J. Yadav, K. Ramineni, M. A. Pericàs, *Org. Lett.* **2016**, *18*, 1602 – 1605; d) J. Izquierdo, M. A. Pericàs, *ACS Catal.* **2016**, *6*, 348 – 356; e) A. E. Fernandes, O. Riant, K. F. Jensen, A. M. Jonas, *Angew. Chem. Int. Ed.* **2016**, *55*, 11044 – 11048; *Angew. Chem.* **2016**, *128*, 11210 – 11214; f) R. P. Jumde, A. Mandoli, *ACS Catal.* **2016**, *6*, 4281 – 4285; g) S. Wang, C. Rodríguez-Escrich, M. A. Pericàs, *Angew. Chem. Int. Ed.* **2017**, *56*, 15068 – 15072; *Angew. Chem.* **2017**, *129*, 15264 – 15268; h) S. Wang, J. Izquierdo, C. Rodríguez-Escrich, M. A. Pericàs, *ACS Catal.* **2017**, *7*, 2780 – 2785; i) R. M. Neyyappadath, R. Chisholm, M. D. Greenhalgh, C. Rodríguez-Escrich, M. A. Pericàs, G. Hähner, A. D. Smith, *ACS Catal.* **2018**, *8*, 1067 – 1075; j) W. Yu, M. Zhou, T. Wang, Z. He, B. Shi, Y. Xu, K. Huang, *Org. Lett.* **2017**, *19*, 5776 – 5779.

[13] a) J. M. Notestein, A. Katz, *Chem. Eur. J.* **2006**, *12*, 3954 – 3965; b) J.-K. Lee, M. Kung, H. Kung, *Top. Catal.* **2008**, *49*, 136 – 144; c) F.-X. Felpin, E. Fouquet, *ChemSusChem* **2008**, *1*, 718 – 724; d) E. L. Margelefsky, R. K. Zeidan, M. E. Davis, *Chem. Soc. Rev.* **2008**, *37*, 1118 – 1126; e) S. Shylesh, W. R. Thiel, *ChemCatChem* **2011**, *3*, 278 – 287; f) U. Díaz, D. Brunel, A. Corma, *Chem. Soc. Rev.* **2013**, *42*, 4083 – 4097; g) N. A. Brunelli, C. W. Jones, *J. Catal.* **2013**, *308*, 60 – 72; h) K. Motokura, *ChemCatChem* **2014**, *6*, 3067 – 3068; i) Y.-B. Huang, J. Liang, X.-S. Wang, R. Cao, *Chem. Soc. Rev.* **2017**, *46*, 126 – 157.

[14] a) P. Chandra, A. M. Jonas, A. E. Fernandes, *ACS Catal.* **2018**, *8*, 6006 – 6011; b) P. Chandra, A. M. Jonas, A. E. Fernandes, *J. Am. Chem. Soc.* **2018**, *140*, 5179 – 5184; c) A. E. Fernandes, A. M. Jonas, *Catal. Today* https://doi.org/10.1016/j.cattod.2018.11.040.

[15] A. E. Fernandes, O. Riant, A. M. Jonas, K. F. Jensen, *RSC Adv.* **2016**, *6*, 36602 – 36605.

[16] a) E.-H. Ryu, Y. Zhao, *Org. Lett.* **2005**, *7*, 1035 – 1037; b) C. Ornelas, J. Ruiz, L. Salmon, D. Astruc, *Adv. Synth. Catal.* **2008**, *350*, 837 – 845; c) C. Ornelas, A. K. Diallo, J. Ruiz, D. Astruc, *Adv. Synth. Catal.* **2009**, *351*, 2147 – 2154; d) V. Rodionov, H. Gao, S. Scroggins, D. A. Unruh, A.-J. Avestro, J. M. J. Fréchet, *J. Am. Chem. Soc.* **2010**, *132*, 2570 – 2572; e) A. T. Dickschat, F. Behrends, M. Bühner, J. Ren, M. Weiß, H. Eckert, A. Studer, *Chem. Eur. J.* **2012**, *18*, 16689 – 16697; f) C. Monasterolo, M. Ballestri, G. Sotgiu, A. Guerrini, P. Dambruoso, K. Sparnacci, M. Laus, M. D. Cesare, A. Pistone, G. L. Beretta, F. Zunino, V. Benfenati, G. Varchi, *Bioorg. Med. Chem.* **2012**, *20*, 6640 – 6647; g) K. Ouadahi, E. Allard, B. Oberleitner, C. Larpent, *J. Polym. Sci. Part A* **2012**, *50*, 314 – 328; h) H. T. Le, H. M. Jeon, C. W. Lim, T. W. Kim, *Carbohydr. Res.* **2014**, *391*, 22 – 28.

[17] J. Zhang, H. Gu, X. Yang, M. Chen, Z. Yang, W. Zhang, *RSC Adv.* **2015**, *5*, 8537 – 8543.

[18] J.-L. M. Abboud, C. Foces-Foces, R. Notario, R. E. Trifonov, A. P. Volovodenko, V. A. Ostrovskii, I. Alkorta, J. Elguero, *Eur. J. Org. Chem.* **2001**, *16*, 3013 – 3024.

[19] M. Vafaeezadeh, M. M. Hashemi, *Chem. Eng. J.* **2014**, *250*, 35 – 41.

[20] M. M. Obadia, B. P. Mudraboyina, A. Serghei, D. Montarnal, E. Drockenmuller, *J. Am. Chem. Soc.* **2015**, *137*, 6078 – 6083.

[21] a) A. Gissibl, M. G. Finn, O. Reiser, *Org. Lett.* **2005**, *7*, 2325 – 2328; b) A. Bastero, D. Font, M. A. Pericàs, *J. Org. Chem.* **2007**, *72*, 2460 – 2468.

[22] a) Z. Yacob, J. Liebscher in *Chemistry of 1,2,3-Triazolium Salts* (Eds.: W. Dehaen, V. A. Bakulev), Springer International Publishing, Cham, **2015**, pp. 167 – 210; b) M. M. Obadia, E. Drockenmuller, *Chem. Commun.* **2016**, *52*, 2433 – 2450.

[23] a) Z. Yacob, J. Shah, J. Leistner, J. Liebscher, *Synlett* **2008**, *15*, 2342 – 2344; b) S. Hanelt, J. Liebscher, *Synlett* **2008**, *7*, 1058 – 1060; c) J. Shah, S. S. Khan, H. Blumenthal, J. Liebscher, *Synthesis* **2009**, *23*, 3975 – 3982; d) L. Li, J. Wang, T. Wu, R. Wang, *Chem. Eur. J.* **2012**, *18*, 7842 – 7851; e) C. J. Whiteoak, A. H. Henseler, C. Ayats, A. W. Kleij, M. A. Pericas, *Green Chem.* **2014**, *16*, 1552 – 1559.

[24] a) A. C. Cole, J. L. Jensen, I. Ntai, K. L. T. Tran, K. J. Weaver, D. C. Forbes, J. H. Davis, *J. Am. Chem. Soc.* **2002**, *124*, 5962 – 5963; b) K. Qiao, H. Hagiwara, C. Yokoyama, *J. Mol. Catal. A* **2006**, *246*, 65 – 69; c) Y. Jeong, D.-Y. Kim, Y. Choi, J.-S. Ryu, *Org. Biomol. Chem.* **2011**, *9*, 374 – 378; d) B. Zhen, Q. Jiao, Y. Zhang, Q. Wu, H. Li, *Appl. Catal. A* **2012**, *445 – 446*, 239 – 245; e) S. M. Vahdat, M. A. Zolfigol, S. Baghery, *Appl. Organomet. Chem.* **2016**, *30*, 311 – 317.

[25] a) Y. Gu, F. Shi, Y. Deng, *J. Mol. Catal. A* **2004**, *212*, 71 – 75; b) H. Xing, T. Wang, Z. Zhou, Y. Dai, *Ind. Eng. Chem. Res.* **2005**, *44*, 4147 – 4150; c) H. Xing, T. Wang, Z. Zhou, Y. Dai, *J. Mol. Catal. A* **2007**, *264*, 53 – 59; d) Y. Zhao, J. Long, F. Deng, X. Liu, Z. Li, C. Xia, J. Peng, *Catal. Commun.* **2009**, *10*, 732 – 736; e) L. Zhang, M. Xian, Y. He, L. Li, J. Yang, S. Yu, X. Xu, *Bioresour. Technol.* **2009**, *100*, 4368 – 4373; f) Q. Zhang, J. Luo, Y. Wei, *Green Chem.* **2010**, *12*, 2246 – 2254; g) Q. Zhang, H. Su, J. Luo, Y. Wei, *Green Chem.* **2012**, *14*, 201 – 208; h) A. S. Amarasekara, *Chem. Rev.* **2016**, *116*, 6133 – 6183.

[26] Z. Fei, D. Zhao, T. J. Geldbach, R. Scopelliti, P. J. Dyson, *Chem. Eur. J.* **2004**, *10*, 4886 – 4893.

[27] K. Song, H. Zhang, Y. Zhang, Y. Tang, K. Tang, *J. Catal.* **2013**, *299*, 119 – 128.

[28] I. Díaz, C. Márquez-Alvarez, F. Mohino, J. N. Pérez-Pariente, E. Sastre, *J. Catal.* **2000**, *193*, 283 – 294.

[29] a) M. S. Azam, S. L. Fenwick, J. M. Gibbs-Davis, *Langmuir* **2011**, *27*, 741 – 750; b) A. T. Dickschat, F. Behrends, S. Surmiak, Y. Wei, H. Eckert, A. Studer, *Chem. Commun.* **2013**, *49*, 2195 – 2197; c) A. T. Dickschat, S. Surmiak, A. Studer, *Synlett* **2013**, *24*, 1523 – 1528; d) L. Deiana, L. Ghisu, S. Afewerki, O. Verho, E. V. Johnston, N. Hedin, Z. Bacsik, A. Córdova, *Adv. Synth. Catal.* **2014**, *356*, 2485 – 2492; e) S. K. Surmiak, C. Doerenkamp, P. Selter, M. Peterlechner, A. H. Schafer, H. Eckert, A. Studer, *Chem. Eur. J.* **2017**, *23*, 6019 – 6028.

[30] E. L. Margelefsky, A. Bendjériou, R. K. Zeidan, V. Dufaud, M. E. Davis, *J. Am. Chem. Soc.* **2008**, *130*, 13442 – 13449.

[31] a) A. A. Nevzorov, *J. Magn. Reson.* **2011**, *209*, 161 – 166; b) J. Raya, B. Perrone, J. Hirschinger, *J. Magn. Reson.* **2013**, *227*, 93 – 102; c) R. L. Johnson, K. Schmidt-Rohr, *J. Magn. Reson.* **2014**, *239*, 44 – 49.

[32] B. M. Fung, A. K. Khitrin, K. Ermolaev, *J. Magn. Reson.* **2000**, *142*, 97 – 101.

Manuscript received: December 13, 2018
Accepted manuscript online: March 15, 2019
Version of record online: April 5, 2019